



**HAL**  
open science

## Wave mixing efficiency in InAs/GaAs semiconductor quantum dot optical amplifiers and lasers

Thibaut Renaud, Heming Huang, Frédéric Grillot, Dieter Bimberg

► **To cite this version:**

Thibaut Renaud, Heming Huang, Frédéric Grillot, Dieter Bimberg. Wave mixing efficiency in InAs/GaAs semiconductor quantum dot optical amplifiers and lasers. *Laser Physics Letters*, 2022, 19 (11), pp.1-6. 10.1088/1612-202x/ac9595 . hal-04555396

**HAL Id: hal-04555396**

**<https://telecom-paris.hal.science/hal-04555396>**

Submitted on 25 Apr 2024

**HAL** is a multi-disciplinary open access archive for the deposit and dissemination of scientific research documents, whether they are published or not. The documents may come from teaching and research institutions in France or abroad, or from public or private research centers.

L'archive ouverte pluridisciplinaire **HAL**, est destinée au dépôt et à la diffusion de documents scientifiques de niveau recherche, publiés ou non, émanant des établissements d'enseignement et de recherche français ou étrangers, des laboratoires publics ou privés.

## Letter

# Wave mixing efficiency in InAs/GaAs semiconductor quantum dot optical amplifiers and lasers

Thibaut Renaud<sup>1,\*</sup>, Heming Huang<sup>1</sup>, Frédéric Grillot<sup>1,2</sup> and Dieter Bimberg<sup>3,4</sup><sup>1</sup> LTCI, Télécom Paris, Institut Polytechnique de Paris, 19 Place Marguerite Perey, 91120 Palaiseau, France<sup>2</sup> Center for High Technology Materials, The University of New-Mexico, Albuquerque, NM 87106, United States of America<sup>3</sup> Center for Nanophotonics, Institute for Solid State Physics, Technische Universität Berlin, Berlin, Germany<sup>4</sup> ‘Bimberg Chinese-German Center for Green Photonics’ of the Chinese Academy of Sciences at CIOMP, Changchun, People’s Republic of ChinaE-mail: [thibaut.renaud@telecom-paris.fr](mailto:thibaut.renaud@telecom-paris.fr)

Received 28 July 2022

Accepted for publication 22 September 2022

Published 7 October 2022

**Abstract**

The nonlinear features of both semiconductor optical amplifiers (SOAs) and semiconductor lasers, which are made from the same InAs/GaAs quantum dot (QD) wafers, are investigated in detail. By employing pump-probe driven four-wave mixing as an experimental tool, the wave conversion process shows notably different profiles for the two types of devices. Due to the contributions of ultrafast, sub-picosecond mechanisms, such as carrier heating and spectral hole burning, the pump-probe frequency can be easily tuned to the THz range. SOAs generally benefit more from sub-picosecond carrier dynamics, hence exhibiting a higher conversion efficiency (CE) in the THz range, compared to their laser diode counterparts. The discrepancy even exceeds 10 dB. In addition, laser experiments yield some differences from the amplifier ones, hence leading to a higher nonlinear CE at small detuning ranges. These results strongly improve our insight into the fundamental nonlinear properties of InAs/GaAs QD material, and contribute to the conception of novel devices for future on-chip applications in all-optical communication networks, such as signal wavelength conversion, mode-locking, and optical frequency comb generation.

Keywords: quantum dots, four wave mixing, optical nonlinearities

(Some figures may appear in colour only in the online journal)

**1. Introduction**

Self-assembled semiconductor quantum dots (QDs) are nano-scale structural clusters with atom-like behavior [4]. Owing

to the three-dimensional spatial quantization, QD materials exhibit advantageous properties for novel energy efficient devices [2, 5, 22] that are inherited from the discretized profiles of their density of states. One of their important features is their ultrafast nonlinear dynamics [2, 3, 22]. Thanks to the ultra-fast carrier relaxation channels from the reservoir to the ground (GS) and excited states (ES) the gain

\* Author to whom any correspondence should be addressed.

recovery of QD devices is much faster than their quantum-well counterparts [6, 24]. Subsequently, QD materials show large nonlinear susceptibilities [11] that are highly beneficial for a variety of applications in devices. For instance, driven by four-wave mixing (FWM), cross-gain modulation [18], wavelength conversion [17], passive mode-locking [2, 15, 22], as well as frequency comb generation [2, 13, 15, 22] have demonstrated exceptional performance.

FWM describes the generation of two additional waves, or wavelength conversion, when two incident waves, referred as pump and probe, are propagating within a gain medium exhibiting a third order nonlinear susceptibility ( $\chi^{(3)}$ ). In semiconductor gain media, FWM is mainly governed by three dominant mechanisms: carrier density pulsations (CDPs), an interband relaxation process induced by the pump-probe beating which lays out a temporal grating in the device, as well as carrier heating (CH) and spectral-hole burning (SHB). These last two mechanisms are contributed by sub-picosecond relaxation mechanism driven by carrier-phonon and carrier-carrier scattering [20, 24]. While CDP leads to a higher conversion rate when pump and probe are relatively close in frequency, CH and SHB are responsible for conversion when the probe is largely detuned from the pump. Therefore, investigating the profile of the FWM conversion efficiency (CE), allows us to study in depth the nonlinear gain properties of the QD semiconductor material. In this work, FWM is used as an experimental tool to compare optical nonlinearities of semiconductor optical amplifiers (SOAs) and semiconductor lasers based on the same indium arsenide / gallium arsenide (InAs/GaAs) QD material. The CE measurements show rather unexpected results: SOAs generally benefit more from sub-picosecond carrier dynamics (stronger contributions from both CH and SHB), hence exhibiting a higher CE in the THz range, compared to their laser diode counterparts, and the discrepancy can even exceed 10 dB. Our results yield important insights to the differences between the two types of components on the level of fundamental physics, and will contribute to the conception of novel QD devices for future on-chip functionalities.

## 2. Description of the QD devices

Our devices are all based on the same InAs/GaAs QDs wafers, and processed using identical technologies. The structure is grown on a n+ doped GaAs (100) substrate by molecular beam epitaxy. The dots were formed on GaAs at 485 °C by depositing 2.5 MLs (monolayers) of InAs at a growth rate of 0.083 ML s<sup>-1</sup> and then covered with a 5 nm thick In<sub>0.15</sub>Ga<sub>0.85</sub>As layer. Ten InAs dot sheets are stacked but separated by p-doped 33 nm GaAs spacers (for more details see [2, 22]). The dots are ~5 nm in vertical and 15 ~ 20 nm in lateral extension, with an areal density of 3 ~ 5 × 10<sup>10</sup> cm<sup>-2</sup>. The waveguide is etched through the active region to provide better current injection efficiency and better optical confinement. The etching can be either deep to increase the optical confinement, or shallow to decrease waveguide losses. Further details regarding the structure and processing can be found elsewhere

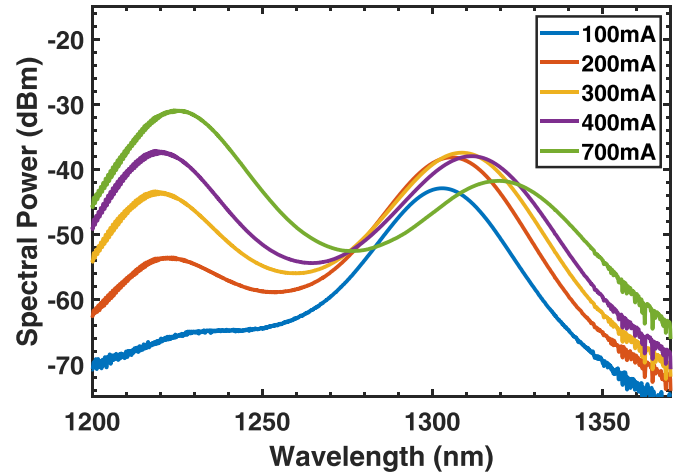


Figure 1. ASE optical spectra captured at different bias currents for the 5 mm SOA.

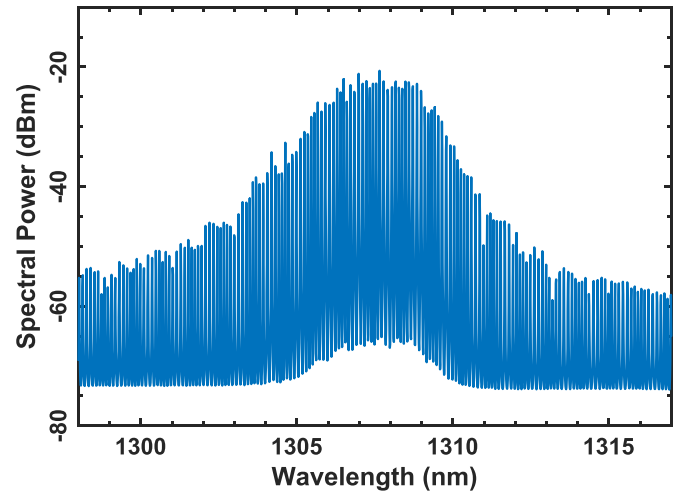
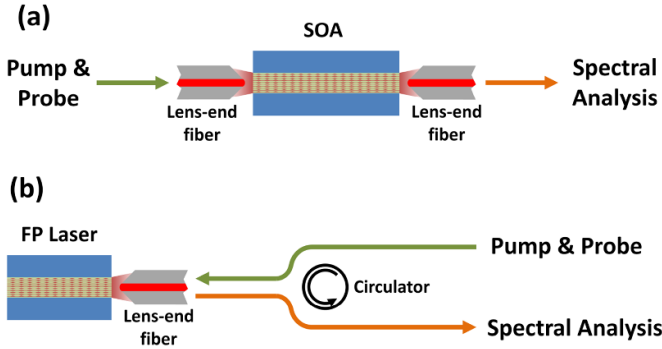


Figure 2. Optical spectrum of the FP laser under  $2 \times I_{th}$  bias at room temperature.

[2, 17, 18, 22]. Results for three SOAs with different lengths are presented here, as well as for one Fabry–Perot (FP) single section laser that can be further used for mode-locking applications. All four devices are biased to operate on the GS. The first SOA has a 2 mm long cavity with a 4 μm wide deep-etched ridge waveguide, while the two other are respectively 3 and 5 mm long, with 4 μm wide shallow-etched waveguides. Figure 1 shows the ASE optical spectra taken at different currents for the 5 mm SOA around room temperature (23 °C). At low currents, the emission is mostly on the GS (around 1308 nm), and at higher currents an ES emission occurs (around 1220 nm).

The FP laser has a cleaved, 2 mm long cavity, with a 2 μm wide ridge waveguide. At room temperature, the threshold current  $I_{th}$  is around 32 mA. Figure 2 depicts the free-running optical spectrum taken at  $2 \times I_{th}$ . At this level, the laser operates on the GS, and the emission is centered around 1308 nm.



**Figure 3.** Experimental setups for (a) SOA device and (b) FP laser device.

### 3. FWM experimental configuration

To investigate FWM, two incident waves, a pump and a probe, are required. In our study, we employed two external cavity tunable lasers to serve that purpose. The pump wavelengths are chosen as the peak of the gain of the ground state, as shown for example in figure 1 for the 5 mm long SOA and figure 2 for the FP laser. The output powers of the pump laser and the probe laser remained constant at respectively 15 and 5 mW (not withstanding coupling losses). The bias currents were chosen similarly to maximize the gain peak of the ground state. Schematics of the experimental setups for both SOA and FP laser are shown in figure 3. The arrows mark the traveling direction of the light within the fibers and devices. Emissions of the two tunable sources are combined using a fiber coupler, and then injected into the active region of each device. One can easily notice the disparity in test-beds for these two component types. In the case of SOA (figure 3(a)), the photons travel throughout the active region without any roundtrip, thus the optical injection is performed with lens-end anti-reflection coated fiber on one side, and the mixed waves are coupled on the other side to the same type of lens-end fiber, before being sent to an optical spectrum analyzer. For the FP laser however (figure 3(b)), thanks to the resonant nature of the cavity, instead of this one-way-across configuration, it is possible to inject and collect light on one side by using an optical circulator, leading to a more concise reflection-based configuration, as only one fiber coupling needs to be monitored. Furthermore, as the collected light has mostly traveled at least one roundtrip in the laser cavity, the interaction length is then no less than double the cavity length (4 mm), which is then comparable with the 5 mm SOA.

### 4. Results and discussion

Figure 4 represents the FWM optical spectrum in the 5 mm SOA device. The pump is in the middle around 1290 nm, which is the center wavelength of the gain, while the probe is tuned to the red side, with its converted signal on the blue side at a symmetric position. The second peak on the red side is the conversion from the pump, and the two minor peaks are the secondary conversions of the pump and probes via the first

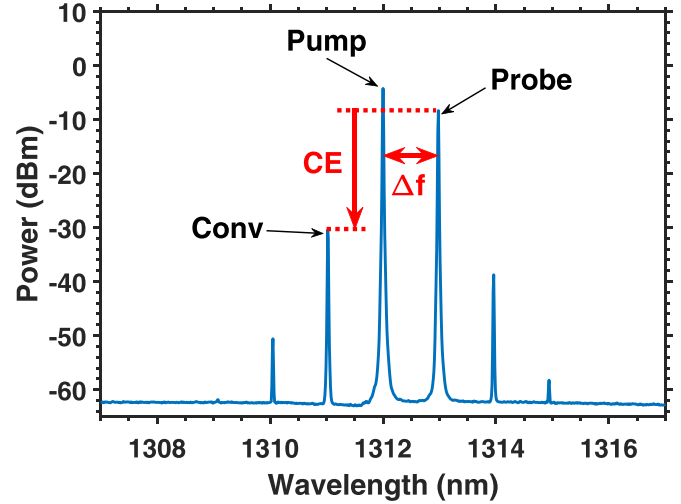


**Figure 4.** FWM optical spectrum in the 5 mm SOA for up-conversion.

converted signals. In this work, we focus only on the first order conversion of the probe by the pump, the others will not be discussed. The frequency detuning  $\Delta f$  is defined as the frequency difference from the probe to the pump ( $f_{\text{probe}} - f_{\text{pump}}$ ). We distinguish wave mixing with  $\Delta f < 0$  from that with  $\Delta f > 0$ . When  $\Delta f < 0$ , the conversion of the probe takes place at higher frequency range, therefore this scenario is referred to as up-conversion in this study, although the probe is located at a lower frequency compared to the pump. For  $\Delta f > 0$ , the conversion is located at a lower frequency, and thus this scenario is referred to as down-conversion. The CE  $\eta_{\text{CE}}$  is then evaluated

$$\eta_{\text{CE}} = \frac{P_{\text{conv}}}{P_{\text{probe}}} \quad (1)$$

where the power of the probe  $P_{\text{probe}}$  and its conversion  $P_{\text{conv}}$  are extracted from the optical spectra. In some studies [14, 19], the definition of CE may differ, with  $P_{\text{probe}}$  taken at the input facet ( $P_{\text{probe}}(0)$ ) instead of at the output facet ( $P_{\text{probe}}(L)$ ), yet, in our case, we only see very few dB difference between the two methods, and the general CE profile remains the same. Thus, we only consider in this work  $P_{\text{probe}}(L)$ , i.e.  $P_{\text{probe}}$  measured from the output spectra. We must point out, CE can be employed as an indicator to evaluate the candidacy of a component as a wavelength converter for communication systems [1, 7, 8, 20], where  $\eta_{\text{CE}}$  is usually calculated with the output power of the probe source as  $P_{\text{probe}}$ ; nevertheless, our main interest in this study, as mentioned earlier, is to probe into the nonlinear properties of the gain media in question, therefore we interpret  $\eta_{\text{CE}}$  directly from the optical spectra at the output of the component. Here,  $\eta_{\text{CE}}$  calculated from figure 4 is  $-22$  dB with  $\Delta f = -180$  GHz, i.e. an up-conversion scenario.

Upon checking the FWM in a FP laser, further adjustment are prerequisite, since generating frequency conversion by the same straightforward manner as in an SOA will not simply

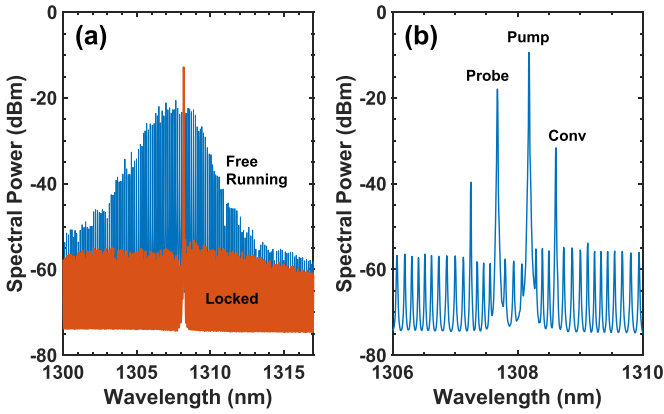


**Figure 5.** (a) Optical spectra of the FP laser in free-running (blue) and after optical injection locking (orange); (b) FWM optical spectrum in FP laser for down-conversion.

work due to the presence of FP modes. To control the interference from the cavity resonances, an optical injection-locking technique is employed to first lock the FP laser on one selected FP mode and suppress all other side modes. This single lasing mode provides the pump in the gain region. Figure 5(a) depicts the optical spectrum of the FP laser before (blue) and after (orange) injection locking. The selected mode is the highest one at the center (1308.18 nm), with a side mode suppression ratio above 40 dB. At this stage, the pump wave is provided by the optical injection locked FP laser [18]. Here the probe cannot be tuned continuously through the spectrum, but needs to coincide with one residual FP mode (after locking). Thus the conversion does not fall in between modes and drops to the noise floor due to destructive interference of the cavity resonance. If the probe conversion coincides with FP mode (done by fine tuning), it can benefit from constructive interference on top of the optical gain. Figure 5(b) depicts a down-conversion spectrum of the FP laser, with  $\Delta f = 89$  GHz and  $\eta_{CE} = -13.7$  dB.

Based on these configurations, the CE is plotted for each device by increasing the frequency detuning from a couple of tens of GHz until the converted signal is no longer visible in the optical spectra. Figure 6 depicts the CE measured as a function of the detuning for the SOAs of three different lengths. The overall profiles are quite similar for all devices: the conversion starts at a high efficiency level, then with the probe being tuned further away from the pump, the intensity of the converted signal decays and merges gradually with the background ASE level. Furthermore, one can notice that two small kinks can be found on each curve around 100 GHz and 1 THz, especially in the up-conversion sets. These two regions are related to the switch of the dominant mechanism that is driving the conversion [18, 20]: while pump and probe remain close, i.e.  $\Delta f < 100$  GHz. The main contribution comes from CDP, and at this stage, the corresponding carrier relaxation time is of the order of a few ps. When  $\Delta f$  extends to a few hundred GHz, CDP can no longer catch up, and CH which is of the order of 100 fs, takes the lead in governing the conversion. Finally, when the pump-probe detuning reaches the THz domain, CH cannot follow either, hence the driving force is

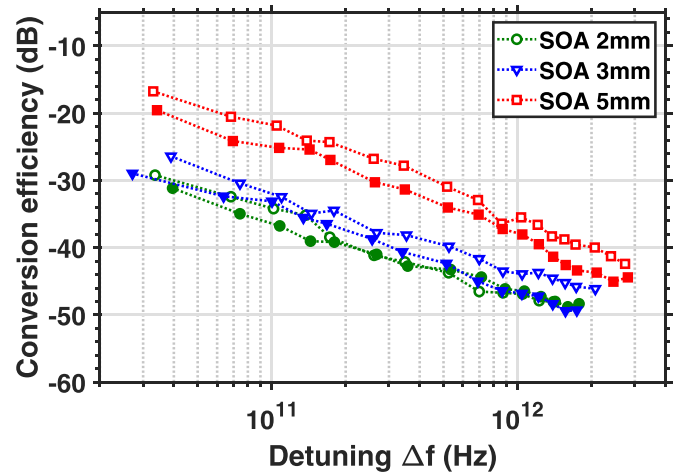


**Figure 6.** Conversion efficiency (in dB) versus detuning in frequency between the two input lasers (in Hz) for the three SOAs. Hollow markers represent up-conversion ( $\Delta f < 0$ ) and solid markers represent down-conversion ( $\Delta f > 0$ ).

due to carrier-carrier scattering, which is the fastest mechanism, with a time constant of the order of 70 fs.

When comparing  $\eta_{CE}$  between different SOAs, upon first glance, it is logical, that with the increase of the longitudinal dimension of the active region, the overall amplitude is magnified almost everywhere within the accessible frequency detuning range, since contributions from CDP, CH and SHB keep accumulating through the light field propagation. Yet, by taking a closer look, the efficiency improvement does not appear quite linear: for the 2 mm gain medium, the maximum frequency detuning  $\Delta f_{max}$  varies from 1.8 THz to 1.4 THz between down- and up-conversion, while  $\eta_{CE}$  tops at  $-29$  dB. In the 3 mm SOA,  $\Delta f_{max}$  is only increased by respectively 40 GHz and 0.7 THz for down- and up-conversion, and the maximal  $\eta_{CE}$  increases by 2.8 dB. Finally, for the 5 mm SOA, the conversion is largely increased, not only the down- and up-conversion are both driven  $\sim 1$  THz further, but also the  $\eta_{CE}$  gains more than 10 dB everywhere within the experimental range. All these improvements are mainly attributed to the longer interaction length for pump and probe fields in the gain media. We also need to point out that the asymmetry between down and up-conversion in SOAs is small. The difference between each set of curves remains constantly below 4 dB. Such closeness is commonly not manifested in laser devices [11, 12, 16, 21, 23], which will be further discussed shortly after.

Figure 7 shows the CE of the 5 mm SOA and the FP laser with regards to the pump-probe frequency detuning. The gap between the two branches in each set highlights the level of symmetry between up-conversion and down-conversion for the two types of devices. The conversion appears to be more symmetrical in the case of the SOAs, both curves being almost superimposed in each set (see also figure 6). Conversely, a gap of  $\sim 10$  dB can be observed for the FP laser. This difference results from sub-picosecond carrier dynamics in optical amplifiers, hence exhibiting a higher CE in the THz range as well as a smaller phase-amplitude coupling, which improves

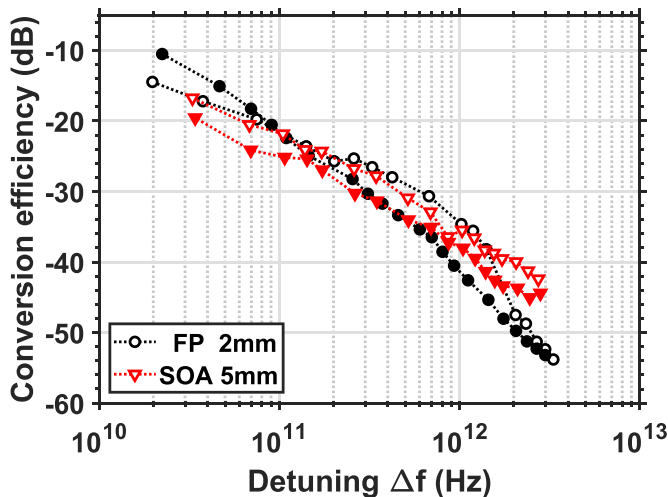


**Figure 7.** Conversion efficiency (in dB) versus detuning in frequency between the two input lasers (in Hz) for the 5 mm SOA and the FP laser. Hollow markers represent up-conversion ( $\Delta f < 0$ ) and solid markers represent down-conversion ( $\Delta f > 0$ ).

the conversion symmetry [1]. Surprisingly, a larger CE is even observed for the 2 mm long laser cavity at small detunings. Although these differences can be attributed to several physical mechanisms including carrier distribution and gain saturation from the intracavity fields, we believe that FWM performed with QD lasers is different from optical amplifiers. Indeed, it was recently shown both theoretically and experimentally that QD lasers exhibit superior FWM gain which is widely amplified by the laser cavity which is meaningful for achieving self-mode-locking and efficient comb sources [9, 10].

## 5. Conclusion

These results highlight clear differences in the nonlinear characteristics between lasers and optical amplifiers. To do so, pump-probe measurements are performed to account for all optical nonlinearities contributing to the FWM signal. Thus, owing to their sub-picosecond carrier dynamics, SOAs clearly demonstrate QD amplifying media achieving conversion efficiencies up to  $-16$  dB along with a detectable signal for more than a THz bandwidth. Surprisingly, QD laser cavity made with the same epitaxial material shows an increase in the FWM net gain ( $-10$  dB) at low detunings which means that in this case self-mode locking can possibly occur by FWM [9]. Overall, this work points out that the large nonlinearities in QDs are particularly important for future on-chip applications in all-optical communication networks, such as signal wavelength conversion, mode-locking and optical frequency comb generation [9].

## Acknowledgments

This work has been supported by the Institut Mines-Télecom and the Technische Universität Berlin.

## References

- [1] Akiyama T, Kuwatsuka H, Hatori N, Nakata Y, Ebe H and Sugawara M 2002 Symmetric highly efficient ( $\sim 0$  dB) wavelength conversion based on four-wave mixing in quantum dot optical amplifiers *IEEE Photonics Technol. Lett.* **14** 1139–41
- [2] Arsenijević D and Bimberg D 2017 *Quantum-Dot Mode-Locked Lasers: Sources for Tunable Optical and Electrical Pulse Combs* (Cham: Springer International Publishing) pp 75–106
- [3] Bakonyi Z, Su H, Onishchukov G, Lester L, Gray A, Newell T and Tunnermann A 2003 High-gain quantum-dot semiconductor optical amplifier for 1300 nm *IEEE J. Quantum Electron.* **39** 1409–14
- [4] Bimberg D, Grundmann M and Ledentsov N 1999 *Quantum Dot Heterostructures* (New York: Wiley)
- [5] Bimberg D and Pohl U W 2011 Quantum dots: promises and accomplishments *Mater. Today* **14** 388–97
- [6] Borri P, Schneider S, Langbein W and Bimberg D 2006 Ultrafast carrier dynamics in InGaAs quantum dot materials and devices *J. Opt. A: Pure Appl. Opt.* **8** S33–S46
- [7] D'Ottavi A, Iannone A, Mecozzi A, Scotti S, Spano P, Dall'Ara R, Eckner J and Guekos G 1995 Efficiency and noise performance of wavelength converters based on FWM in semiconductor optical amplifiers *IEEE Photonics Technol. Lett.* **7** 357–9
- [8] D'Ottavi A, Spano P, Hunziker G, Paiella R, Dall'Ara R, Guekos G and Vahala K 1998 Wavelength conversion at 10 Gb/s by four-wave mixing over a 30-nm interval *IEEE Photonics Technol. Lett.* **10** 952–4
- [9] Duan J, Dong B, Chow W W, Huang H, Ding S, Liu S, Norman J C, Bowers J E and Grillot F 2022 Four-wave mixing in 1.3  $\mu\text{m}$  epitaxial quantum dot lasers directly grown on silicon *Photon. Res.* **10** 1264–70
- [10] Grillot F, Chow W W, Dong B, Ding S, Huang H and Bowers J 2022 Multimode physics in the mode locking of semiconductor quantum dot lasers *Appl. Sci.* **12** 3504
- [11] Huang H, Schires K, Poole P J and Grillot F 2015 Non-degenerate four-wave mixing in an optically injection-locked InAs/InP quantum dot Fabry-Perot laser *Appl. Phys. Lett.* **106** 143501
- [12] Ishikawa H, Watanabe S and Kuwatsuka H 1999 Wavelength conversion technologies for photonic network systems *Fujitsu Sci. Tech. J.* **25** 126–38
- [13] Kurczveil G, Seyed M A, Liang D, Fiorentino M and Beausoleil R G 2018 Error-free operation in a hybrid-silicon quantum dot comb laser *IEEE Photonics Technol. Lett.* **30** 71–74
- [14] Kuyken B et al 2011 Nonlinear properties of and nonlinear processing in hydrogenated amorphous silicon waveguides *Opt. Express* **19** B146–53
- [15] Liu S, Jung D, Norman J, Kennedy M, Gossard A and Bowers J 2018 490 fs pulse generation from passively mode-locked single section quantum dot laser directly grown on on-axis GaP/Si *Electron. Lett.* **54** 432–3
- [16] Lu Z, Liu J, Raymond S, Poole P, Barrios P, Poitras D, Sun F, Pakulski G, Bock P and Hall T 2006 Highly efficient non-degenerate four-wave mixing process in InAs/InGaAsP quantum dots *Electron. Lett.* **42** 1112–4
- [17] Meuer C, Schmidt-Langhorst C, Schmeckebier H, Fiol G, Arsenijević D, Schubert C and Bimberg D 2011 40 gb/s wavelength conversion via four-wave mixing in a quantum-dot semiconductor optical amplifier *Opt. Express* **19** 3788–98
- [18] Meuer C, Schmeckebier H, Fiol G, Arsenijević D, Kim J, Eisenstein G and Bimberg D 2010 Cross-gain modulation and four-wave mixing for wavelength conversion in

- undoped and p-doped 1.3- $\mu\text{m}$  quantum dot semiconductor optical amplifiers *IEEE Photon. J.* **2** 141–51
- [19] Monat C, Ebnali-Heidari M, Grillet C, Corcoran B, Eggleton B J, White T P, O’Faolain L, Li J and Krauss T F 2010 Four-wave mixing in slow light engineered silicon photonic crystal waveguides *Opt. Express* **18** 22915–27
- [20] Nielsen D and Chuang S L 2010 Four-wave mixing and wavelength conversion in quantum dots *Phys. Rev. B* **81** 035305
- [21] Sadeev T, Huang H, Arsenijević D, Schires K, Grillot F and Bimberg D 2015 Highly efficient non-degenerate four-wave mixing under dual-mode injection in InP/InAs quantum-dash and quantum-dot lasers at 1.55  $\mu\text{m}$  *Appl. Phys. Lett.* **107** 191111
- [22] Schmeckeber H and Bimberg D 2017 *Quantum-Dot Semiconductor Optical Amplifiers for Energy-Efficient Optical Communication* (Cham: Springer International Publishing) pp 37–74
- [23] Simoyama T, Kuwatsuka H and Ishikawa H 1998 Cavity length dependence of wavelength conversion efficiency of four-wave mixing in  $\lambda/4$ -shifted DFB laser *Fujitsu Sci. Tech. J.* **34** 235–44
- [24] Uskov A V, Meuer C, Schmeckeber H and Bimberg D 2011 Auger capture induced carrier heating in quantum dot lasers and amplifiers *Appl. Phys. Express* **4** 022202